2-28-2023

Zika virus spreads through infection of lymph node-resident macrophages

Glennys V Reynoso

Autumn C Holmes

Yael Alippe

Michael S Diamond

et al.

Cell Reports

Article

Zika virus spreads through infection of lymph node-resident macrophages

Graphical abstract

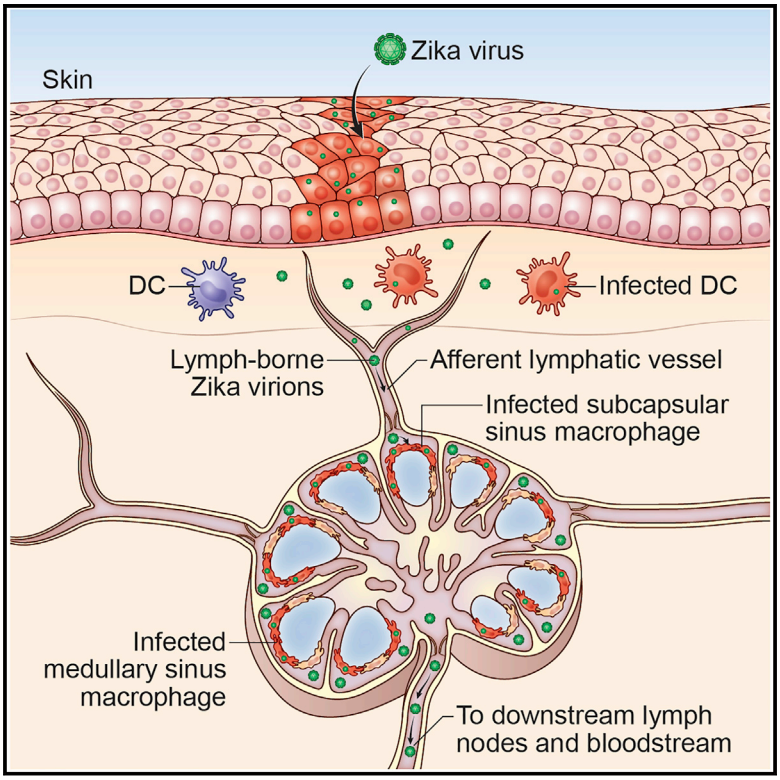

Highlights

- ZIKV infects and replicates in distinct LN macrophage populations
- LN macrophage infection precedes the development of viremia
- Virus reaches the blood in the absence of DC migration or monocyte infection
- CD169^{+} macrophage infection alone does not induce morbidity

Authors

Glennys V. Reynoso, David N. Gordon, Anurag Kalia, ..., Michael S. Diamond, Theodore C. Pierson, Heather D. Hickman

Correspondence

hhickman@mail.nih.gov

In brief

Reynoso et al. show that macrophages in the draining lymph nodes are rapidly infected following footpad inoculation of mice with Zika virus. These nodal macrophages serve as a source of the virus for early ZIKV dissemination.

Reynoso et al., 2023, Cell Reports *42*, 112126
February 28, 2023
https://doi.org/10.1016/j.celrep.2023.112126

Cell Reports

CellPress
OPEN ACCESS

Article

Zika virus spreads through infection of lymph node-resident macrophages

Glennys V. Reynoso,[1] David N. Gordon,[2] Anurag Kalia,[1] Cynthia C. Aguilar,[1] Courtney S. Malo,[1] Maya Aleshnick,[2] Kimberly A. Dowd,[2] Christian R. Cherry,[1] John P. Shannon,[1] Sophia M. Vrba,[1] Autumn C. Holmes,[3] Yael Alippe,[3] Sonia Maciejewski,[2] Kenichi Asano,[4] Michael S. Diamond,[3,5,6,7] Theodore C. Pierson,[2] and Heather D. Hickman[1,8,*]

[1]Viral Immunity and Pathogenesis Unit, Laboratory of Clinical Immunology and Microbiology, National Institute of Allergy and Infectious Diseases (NIAID), National Institutes of Health (NIH), Bethesda, MD, USA

[2]Viral Pathogenesis Section, Laboratory of Viral Diseases (LVD), NIAID, NIH, Bethesda, MD, USA

[3]Department of Medicine, Washington University School of Medicine, St. Louis, MO, USA

[4]Laboratory of Immune Regulation, School of Life Science, Tokyo University of Pharmacy and Life Sciences, Tokyo 192-0392, Japan

[5]Department of Pathology and Immunology, Washington University School of Medicine, St. Louis, MO, USA

[6]Department of Molecular Microbiology, Washington University School of Medicine, St. Louis, MO, USA

[7]The Andrew M. and Jane M. Bursky Center for Human Immunology and Immunotherapy Programs, Washington University School of Medicine, St. Louis, MO, USA

[8]Lead contact

*Correspondence: hhickman@mail.nih.gov

https://doi.org/10.1016/j.celrep.2023.112126

SUMMARY

To disseminate through the body, Zika virus (ZIKV) is thought to exploit the mobility of myeloid cells, in particular monocytes and dendritic cells. However, the timing and mechanisms underlying shuttling of the virus by immune cells remains unclear. To understand the early steps in ZIKV transit from the skin, at different time points, we spatially mapped ZIKV infection in lymph nodes (LNs), an intermediary site *en route* to the blood. Contrary to prevailing hypotheses, migratory immune cells are not required for the virus to reach the LNs or blood. Instead, ZIKV rapidly infects a subset of sessile CD169^{+} macrophages in the LNs, which release the virus to infect downstream LNs. Infection of CD169^{+} macrophages alone is sufficient to initiate viremia. Overall, our experiments indicate that macrophages that reside in the LNs contribute to initial ZIKV spread. These studies enhance our understanding of ZIKV dissemination and identify another anatomical site for potential antiviral intervention.

INTRODUCTION

Flaviviruses are single-stranded, positive-sense RNA viruses that cause a spectrum of severe neurotropic and viscerotropic human diseases and have high epidemic potential.[1] Zika virus (ZIKV) is a mosquito-borne flavivirus that explosively emerged in the Americas in 2015.[2] Although most ZIKV infections during this epidemic were mild and self-limiting, some individuals experienced prolonged viremia with viral RNA detectable in the serum for weeks to months.[3] This epidemic revealed new clinical features of infection, including congenital neurodevelopmental disease and microcephaly.[4] Concerns over ZIKV-induced disease spurred the rapid development of animal models to evaluate ZIKV pathogenesis, vaccine candidates, and therapeutics (reviewed in Shan et al.[5]). Neutralizing antibodies (NAbs) have been identified as a correlate of protection after viral challenge.[6–9] No drugs or vaccines are currently approved for treatment of ZIKV infection.

ZIKV induces pathogenesis after dissemination from the skin into the blood, after which the virus gains access to many different tissues, including the brain and, in pregnant women, the decidua, placenta, and fetus.[10–12] Viral replication in the tissue as well as induction of antiviral immune responses, including type I interferons (IFN-I), can cause tissue damage and fetal demise.[13,14] The importance of dissemination in ZIKV-induced disease has led to investigation of the cellular targets for ZIKV infection and the routes of dissemination into peripheral tissues. The TAM family of receptor tyrosine kinases (including *Tyro3*, *Axl*, and *Mertk* [*TAM*]) were among the first proteins identified that could promote ZIKV infection *in vitro*.[15–17] Because these proteins are highly expressed on endothelial cells,[18] ZIKV infection of vascular endothelial cells via TAM receptors provides one explanation for the ability of ZIKV to access many different tissues from the blood. However, mice deficient in AXL and MERTK expression have been shown to exhibit similar levels of ZIKV infection and viral distribution as wild-type mice.[19] A second possible route for ZIKV movement into the tissues is through mobile immune cells. In human blood, circulating monocytes have been identified as the primary cell type infected by ZIKV, and human monocytes also can be infected *in vitro*.[20–22] Using a ZIKV engineered to only infect myeloid cells, one study showed that monocytes represent the major myeloid population to disseminate ZIKV in mice.[23] Indeed, monocytes are an attractive conduit for viral movement because these cells are abundant in the blood and migrate into even immune-privileged tissues.[24]

Thus, monocytes could serve as "Trojan horses" that distribute ZIKV throughout the body.[22,25] Many other myeloid cells in the skin, including dermal dendritic cells (DCs) and Langerhans cells, also are permissive for ZIKV[23,26–30] and have been proposed to facilitate its dissemination.

Viral dissemination is often viewed as the sum of its products (e.g., cumulative peripheral organ infection) because this is ultimately what results in virus-induced disease. However, dissemination is a complex, multi-step process, and disruption of early dissemination events could prevent or limit downstream viral entry into distant tissues. The cells responsible for early viral movement, particularly within the lymph node (LN), remain unclear. Additionally, it is unknown whether the LN serves to amplify virus draining from the infection site or simply acts as a passageway for virus produced in the skin.

In this study, we examined the early events after ZIKV infection to determine the mechanisms allowing the initial movement of ZIKV from skin to LN to blood. Using mouse models of ZIKV infection, we demonstrate that mobile immune cells do not initially act as Trojan horses of viral distribution while executing their immune functions. Instead, we show that LNs are seeded by ZIKV within minutes of inoculation via lymphatic vessel transport rather than by cellular migration. Moreover, immobile macrophages in the LNs are readily infected by ZIKV before viremia is detectable. Furthermore, viremia can be established without monocyte infection or DC migration from the skin. Thus, LN macrophages are a key link in the chain of ZIKV dissemination that could be targeted by antiviral therapeutics.

RESULTS

ZIKV is captured by the local draining LNs before systemic dissemination

To understand how ZIKV disseminates from the skin, we used an established mouse model of ZIKV infection, footpad inoculation of interferon alpha receptor 1 (*Ifnar1*)$^{-/-}$ mice.[12] Although ZIKV efficiently antagonizes human IFN-I responses, it cannot bind to or inhibit murine STAT2, necessitating circumvention of IFN-I signaling to support murine infection.[31] We first examined the early kinetics of viral delivery to the LN draining the hindfoot, the popliteal LN (PLN), reasoning that we should not detect high levels of virus within an hour if skin cells were needed to replicate the virus (Figure 1). We inoculated mice in the hind footpad with 10^4 focus-forming units (FFUs) of ZIKV H/PF/2013 and harvested PLNs from 5 min to 1 h post infection (p.i.) for infectious viral titers, as determined by a focus formation assay (FFA) (Figure 1A). Within the first hour, we detected infectious ZIKV in PLN homogenates but not in the serum, indicating that the virus reaches the PLN after initial inoculation, likely via the lymphatics. The initial entry of infectious virus in the PLN peaked between 10 and 30 min after inoculation before dropping to levels just above the limit of detection at 1 h.

We next quantified infectious virus in the PLN or serum over a longer period, every 4 h for the first 32 h p.i. (Figure 1B). At 8 h, we did not detect infectious virus in the PLN. However, viral titers rebounded to greater levels than the initial input virus by 16 h p.i. Viremia was detected at 12 h p.i. and was elevated by 16 h p.i. We obtained similar results in wild-type C57BL/6 mice receiving an anti-IFNAR1 Ab (MAR1-5A3, described in Lazear et al.[11]) (Figure S1). In C57BL/6 mice with intact IFN-I signaling, similar levels of infectious virus were measured at the PLN 30 min post-inoculation, but titers never increased, indicating that viral replication drives the higher viral titers seen in the PLN at later time points in *Ifnar1*$^{-/-}$ mice (Figure S1).

The LNs act as a system of sequential filters that remove viruses from the lymph flow.[32] From the PLN, lymph fluid passes to the iliac LN (ILN) and then to the renal LN (RLN) before emptying into the bloodstream via the thoracic duct (depicted in Figure 1C).[33] Thus, the ILN should have the opportunity to sequester virus not captured by the PLN. Infectious virus was not detected in the ILN before 16 h p.i., indicating that the PLN captures virtually all lymph-borne ZIKV at this initial inoculation dose (Figure 1D). Together, these data demonstrate that infectious ZIKV inoculated into the skin via injection passes to the draining LN, where it is captured.

ZIKV replicates in distinct LN macrophage niches

LNs contain at least five distinct populations of macrophages, which form a network to carry out specific immune functions.[34] Macrophages present in nodal sinuses represent an immobile population of phagocytic cells that are situated with their somas in the sinusoidal space and projections through the lymphatic endothelial cells that form the sinus floor and provide cytokines necessary for macrophage survival.[35,36] Sinus-resident macrophages can be subdivided further based on their location within the LN and expression of cell-surface molecules.[37] Sinus-resident macrophages nearest the afferent (incoming) lymph vessel have been termed subcapsular sinus macrophages (SSMs), whereas those nearest the efferent (exiting) lymph vessels are called medullary sinus macrophages (MSMs). These populations access lymph-borne particulates sequentially as lymph enters the node through the subcapsular sinus and flows around to the medullary sinus.[38]

Because of their location, we first investigated whether lymphoid sinus-resident macrophages capture ZIKV. We imaged frozen cross-sections of the PLN harvested from 8–24 h p.i. from C57BL/6 mice, C57BL/6 mice treated with an anti-IFNAR1 Ab, or *Ifnar1*$^{-/-}$ mice (Figure 2). LNs were oriented so that they were sectioned from the top of the LN (near the afferent lymphatics) through the medulla and hilum, as described previously,[39] thus affording a complete view of the major anatomical subdivisions of the LN. We distinguished CD169$^+$ sinusoidal macrophage populations by their location and morphology, as described previously.[37,39,40] At 8 h p.i., we detected ZIKV E protein that colocalized with small patches of SSMs, regardless of the type I IFN signaling capacity of the recipient mice and, thus, likely reflecting binding of the input virus (Figure 2A). We did not detect ZIKV E protein staining in negative control LNs infected with vaccinia virus (VACV), which induces nodal inflammation and increases background Ab staining (Figure S2). We identified ZIKV-infected cells by staining for the non-structural protein NS2b, which is not incorporated into virions (Figures 2B–2D). By 8 h p.i., NS2b staining was detected at low levels in the LN and restricted to SSMs. By 16 h, we detected prominent NS2b staining in MSMs located in medullary sinuses (Figures 2C and 2D). Most of the NS2b-infected cells in *Ifnar1*$^{-/-}$ mice expressed CD11b and SIGNR1,

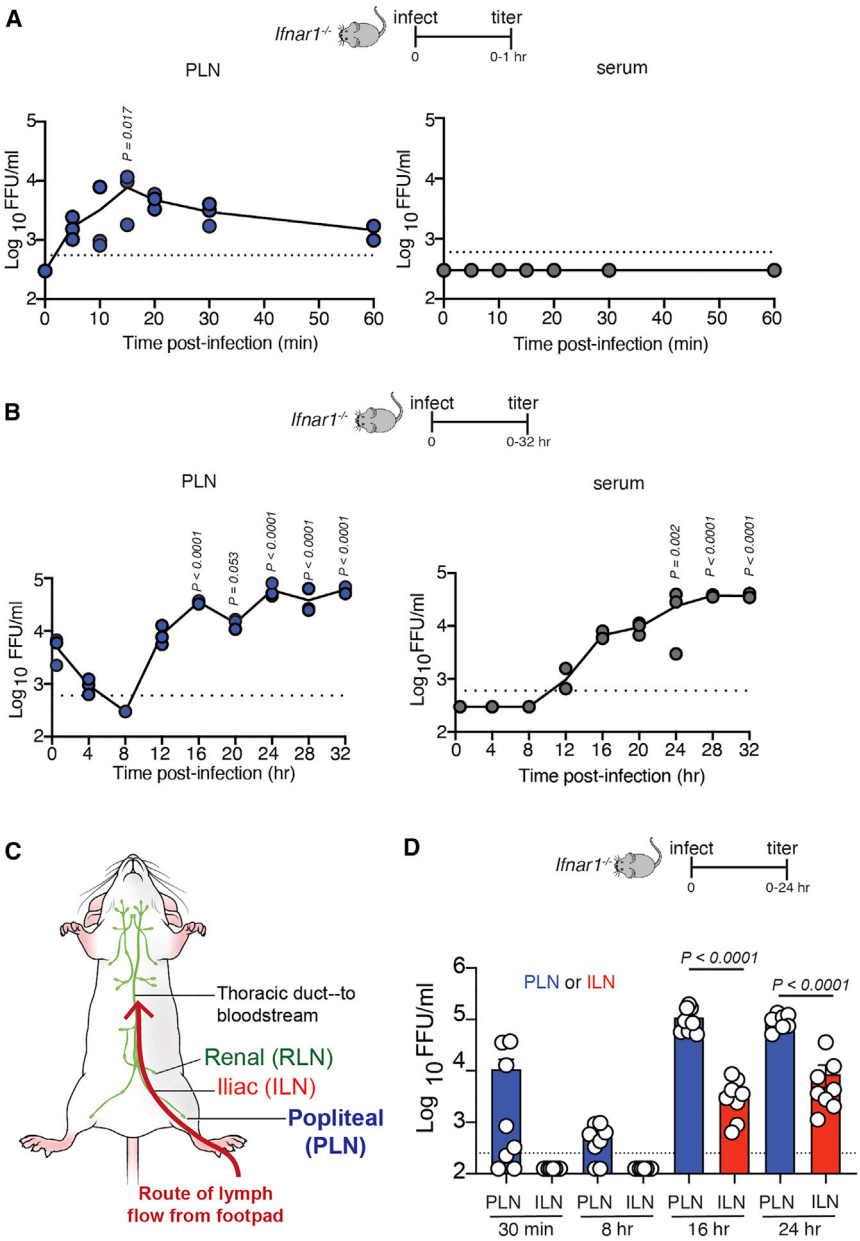

Figure 1. ZIKV replicates in the PLN before systemic dissemination

(A) Viral titers (in focus-forming units [FFUs] per milliliter) in the PLN (left, blue dots) or serum (right, gray dots) harvested at the indicated time (in minutes) during the first hour following footpad (FP) injection of *Ifnar1*$^{-/-}$ mice with 10^4 FFUs of ZIKV H/PF/2013. Dots represent individual mice (either pooled PLNs or separate sera) and the average of technical replicates in the focus formation assay (FFA). A dashed line shows the limit of detection (LOD) of the FFA. Values below the LOD are reported as half the LOD (125 FFU/mL). PLNs and sera were harvested from the same mice. Data are shown from 1 of 2 complete time-course experiments.

(B) Viral titers in the PLN (left, blue dots) or serum (right, gray dots) at the indicated time point during the first 32 h p.i. of *Ifnar1*$^{-/-}$ mice. Data are shown from 1 of 2 complete time-course experiments.

(C) Illustration of the route of lymphatic draining from the FP. Lymph first flows to the popliteal LN (PLN), followed by the iliac LN (ILN). Downstream of the nodes, lymph enters the thoracic duct, followed by the subclavian vein (where it enters the blood).

(D) Viral titers in PLNs (blue bars) and ILNs (red bars) of *Ifnar1*$^{-/-}$ mice at the indicated time p.i. (in hours). PLNs and ILNs were harvested from the same mice. Data are shown from two pooled experiments with 4 mice/group.

All experiments were repeated 2–3 times with 3–4 mice per group. Dots represent individual mice (either pooled LNs or separate sera) and the average of technical replicates in the FFA. Error bars, SEM. Dashed line, LOD for the assay. Statistics, one-way ANOVA. Exact p values are shown in relation to uninfected controls.

but not CD11c, at 16 h p.i., consistent with previous analyses demonstrating a paucity of infected DCs in ZIKV-infected LNs at early time points[39] (Figures S2D–S2F). Staining of the ILN revealed a similar but delayed pattern of infection, with SSMs being productively infected at 16 h p.i., followed by MSMs at 24 h p.i. (Figure S2).

In these studies, both murine models of ZIKV infection utilized mice that were deficient in type I IFN signaling either genetically or through Ab treatment. To understand whether LN macrophages were also infected in a more immunocompetent animal model, we inoculated human STAT2 knockin (*hStat2-KI*) mice with a mouse-adapted strain of ZIKV (MA Dakar), as described previously.[10] Confocal imaging of the PLN 16 h p.i. revealed ZIKV NS2b$^+$ SSMs and MSMs (Figure 2E). Together, these data reveal that, in mice, footpad-inoculated ZIKV transits through and infects LN macrophages.

ZIKV infection disrupts LN macrophages

After inflammatory stimulation by either live or dead virus, SSMs undergo attrition because of inflammasome activation and pyroptosis or through necroptosis.[41–43] We exploited this feature as a surrogate measure of LN-macrophage sensing of lymph-borne ZIKV without a requirement for direct infection. We performed flow cytometry on single-cell suspensions of PLNs or ILNs harvested 72 h p.i. from mice with or without IFN-I signaling (Figures 3A and 3B). We gated on live CD45$^+$CD11c^{lo}CD11b$^+$CD169$^+$ cells and further separated macrophage populations using F4/80 (present on MSMs only[37]). SSMs were absent in the PLN and ILN at this time point; this did not require productive ZIKV infection because SSMs were also ablated in wild-type (WT) mice. In contrast to SSMs, MSMs are not thought to undergo p.i. attrition.[41] However, by 72 h p.i., MSMs were largely absent in *Ifnar1*$^{-/-}$ mice, although some MSMs were still detectable in C57BL/6 mice with intact IFN-I

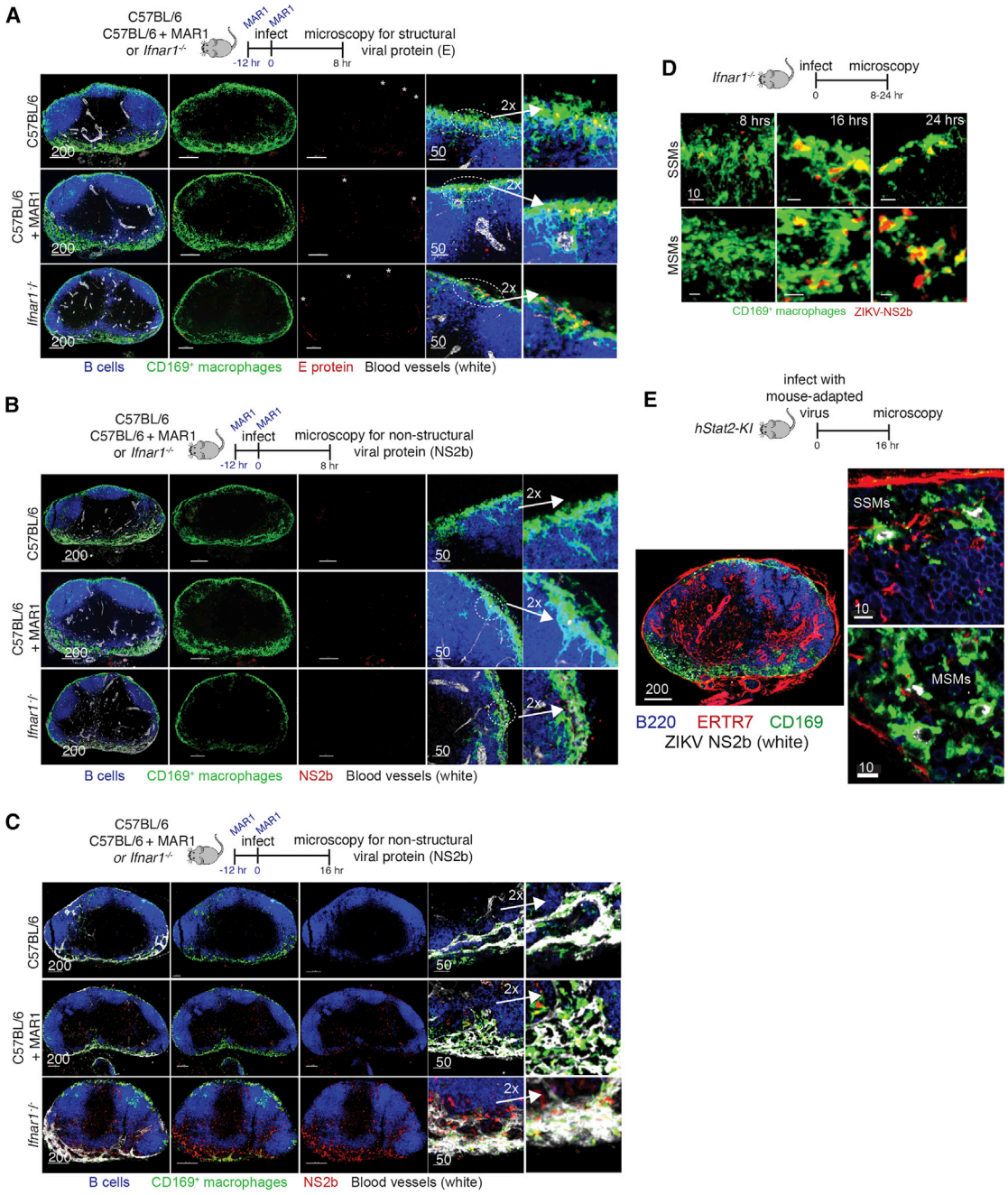

Figure 2. ZIKV infects macrophages in LN sinuses

(A) Confocal images of frozen PLN sections from nodes harvested 8 h p.i. from C57BL/6 mice (top panels), C57BL/6 mice given the anti-IFNAR1 Ab MAR1-5A3 (center panels), and *Ifnar1*$^{-/-}$ mice (bottom panels). Blue, B cells; green, CD169^{+} macrophages; red, ZIKV E protein; white, CD31. The far right panels show a higher-magnification view of the SCS. Dashed ovals show specific areas with ZIKV E protein staining. An asterisk indicates patches of SSMs with E protein staining.

(B) Confocal images of frozen PLN sections from nodes harvested 8 h p.i. from C57BL/6 mice (top panels), C57BL/6 mice given the anti-IFNAR1 Ab MAR1-5A3 (center panels), and *Ifnar1*$^{-/-}$ mice (bottom panels). Blue, B220; green, CD169; red, ZIKV NS2b protein; white, CD31. The far right panel shows a higher-magnification view of the SCS. Dashed ovals show specific areas with ZIKV NS2b protein staining.

(C) As in (B), but PLNs were harvested 16 h p.i.

(D) Confocal images of frozen PLN sections from nodes harvested at the indicated time (shown in hours p.i. in the top right corners) from *Ifnar1*$^{-/-}$ mice. The top panels show macrophages in the SCS (SCS macrophages [SSMs]), and the bottom panels show macrophages in medullary sinuses (MS macrophages [MSMs]). Green, CD169; red, ZIKV NS2b protein.

(E) Confocal images of frozen PLN sections from nodes harvested 16 h p.i. from *hStat2-KI* mice infected with mouse-adapted ZIKV. Green, CD169; red, ERTR-7 (LN stroma); white, ZIKV NS2b protein; blue, B220. Higher-magnification images on the right show NS2b^{+} SSMs (top panel) and MSMs (bottom panel).

Images are representative of 6–10 PLNs/time point/condition harvested from 3–5 mice. Scale bars are in micrometers.

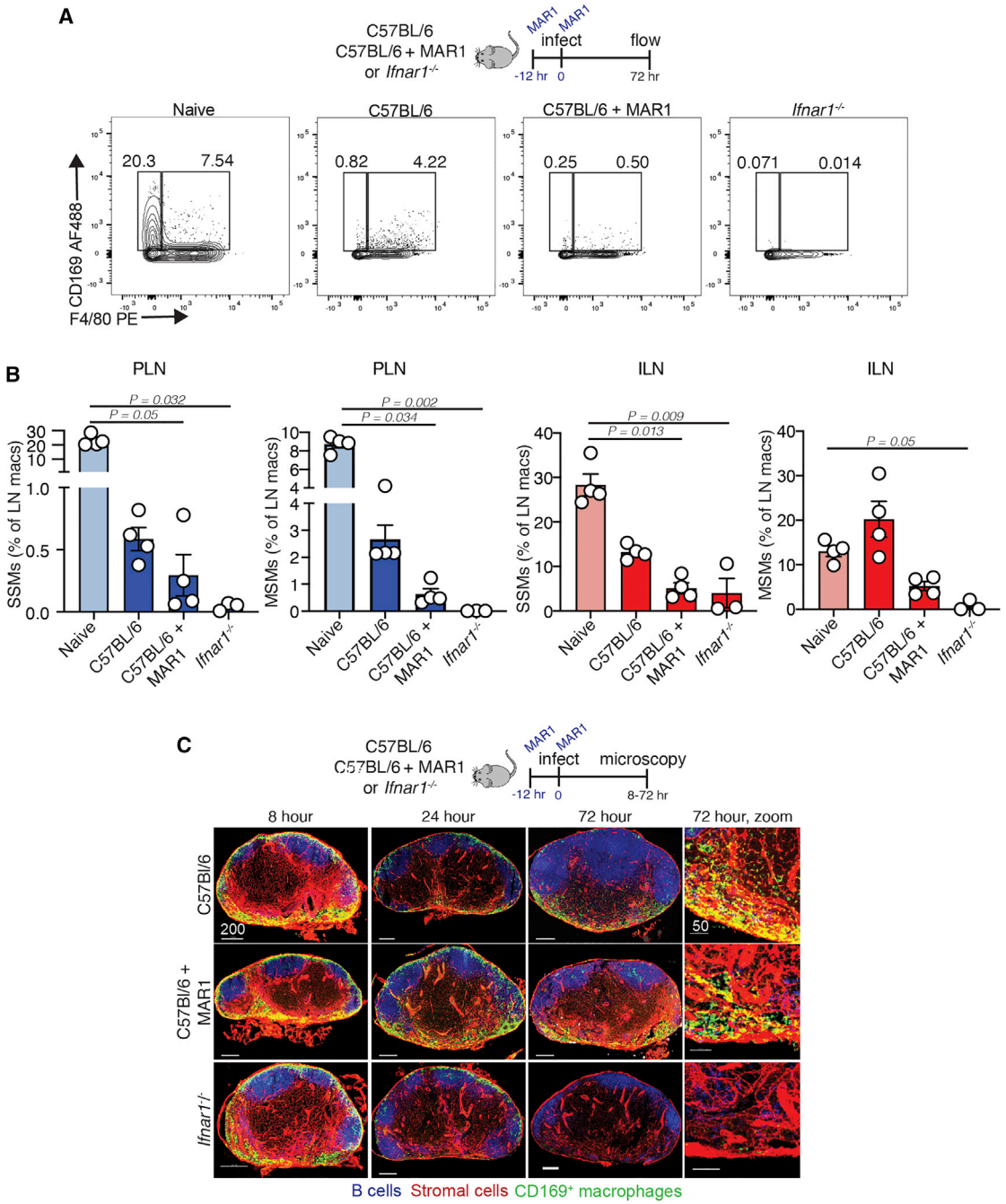

Figure 3. ZIKV disrupts LN macrophage networks

(A) Flow plots generated from single-cell suspensions of PLNs harvested from uninfected C57BL/6 mice (left panel), ZIKV-infected C57BL/6 mice (center left), C57BL/6 + anti-IFNAR1 Ab MAR1-5A3 mice (center right), and *Ifnar1*$^{-/-}$ mice (right) 72 h p.i. Cells were first gated on CD45^{+} B220^{-} CD3^{-} CD11b^{+} CD11c^{low} cells. Gating indicates SSMs (left gates, CD169^{+} F4/80^{-}) and MSMs (right gates, CD169^{+} F4/80^{+}).

(B) Frequency of CD169^{+} SSMs (far left and center right panels) or MSMs (center left and far right panels) in PLNs (blue bars) and ILNs (red bars) as a percentage of total LN macrophages from the experiment shown in flow plots in (A). Statistics, one-way ANOVA. Dots show pooled LNs from individual mice. Error bars, SEM. The experiment was repeated 3 times with 3–4 mice/group.

(C) Confocal images of frozen PLN sections harvested from C57BL/6 mice (top panels), C57BL/6 mice given the anti-IFNAR1 Ab MAR1-5A3 (center panels), or *Ifnar1*$^{-/-}$ mice (bottom panels) at the indicated time p.i. Blue, B cells; green, CD169^{+} macrophages; red, stromal cells (ERTR-7^{+}). The far right panel shows a higher-magnification view of the medullary sinus.

Images in (C) are representative of 6–10 LNs/time point/condition harvested from 3–5 mice. Scale bars are in micrometers.

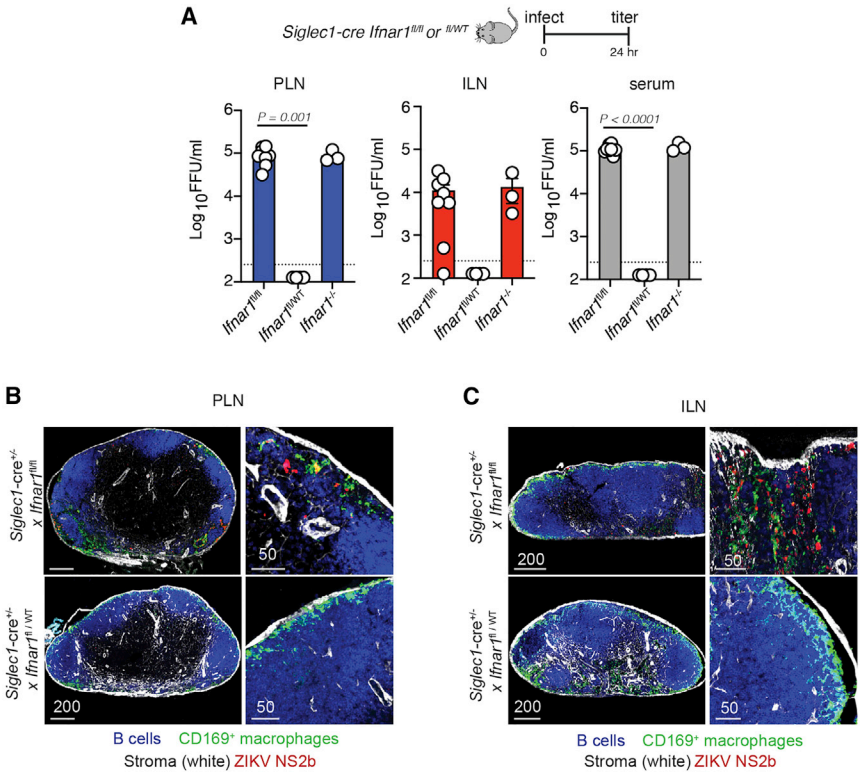

Figure 4. CD169$^+$ macrophage infection supports systemic dissemination

(A) Viral titers (FFUs per milliliter) in the PLN (left, blue bars), ILN (center, red bars), and serum (right, gray bars) harvested 24 h p.i. from *Siglec1-cre Ifnar*$^{fl/fl}$ (homozygous *Ifnar1* knockout in CD169$^+$ cells [cKO]) mice, *Siglec1-cre Ifnar*$^{fl/WT}$ (heterozygous knockout in CD169$^+$ cells), and *Ifnar1*$^{-/-}$ mice with 10^4 FFUs of ZIKV. The experiment was repeated 3 times with 3–4 mice per group. Results shown are pooled from two independent experiments. Dots represent individual mice (either pooled LNs or separate serum) and the average of technical replicates . Dashed line, LOD for the assay. Values below the LOD are reported as half the LOD (125 FFU/mL).

(B) Confocal images of frozen PLN sections harvested 24 h p.i. from *Siglec1-cre Ifnar*$^{fl/fl}$ (homozygous cKO) mice (top panels) and *Siglec1-cre Ifnar*$^{fl/WT}$ (heterozygous cKO mice, bottom panels) stained for B cells (using the B220 Ab, blue), CD169$^+$ macrophages (green), stromal cells (using ERTR7, white), and ZIKV NS2b protein (red). The right panels show higher-magnification images. Scale bars are in micrometers.

(C) As in (B) but showing the ILN instead of PLN.

signaling (Figure 3). The prominent MSM ablation in *Ifnar1*$^{-/-}$ mice indicates that the MSM compartment has access to virus or viral antigen produced after viral replication in these animals.

LN macrophages are difficult to remove by enzymatic tissue dissociation and may be overestimated by flow cytometry approaches because of lymphocyte binding of CD169$^+$ cell debris.[44] As a second measure, we also examined LNs over the same time frame using confocal microscopy (Figure 3C). Imaging at 72 h p.i. recapitulated the SSM and MSM ablation in *Ifnar1*$^{-/-}$ mice observed using flow cytometry. We also noted little overt change in LN architecture, as judged by staining of LN stromal and vascular cells. The LN macrophage network remained largely intact at 8 h and partially intact at 24 h (Figure 3C). Together, these data show that footpad inoculation with ZIKV results in infection and disruption of the PLN macrophage network.

CD169$^+$ macrophage infection alone allows systemic viral dissemination

To more definitively understand the role of LN macrophages in ZIKV dissemination, we crossed *Siglec1-cre* mice (with Cre recombinase expression in CD169$^+$ cells[45]) with *Ifnar1*-floxed mice[46] to conditionally delete IFN-I signaling in CD169$^+$ macrophages (*Siglec1-cre Ifnar1*$^{fl/fl}$ mice, hereafter referred to as CD169 conditional knockout (cKO); Figure 4). Viral titers in the PLN or ILN at 24 h p.i. infection were unexpectedly high even though viral replication was restricted to only CD169$^+$ macrophages (titers were statistically similar to *Ifnar1*$^{-/-}$ mice) (Figure 4A). Moreover, the levels of infectious ZIKV in the serum were similar in *Ifnar1*$^{-/-}$ and CD169 cKO mice, indicating that infection of CD169$^+$ macrophages alone could lead to high levels of disseminated virus by 24 h p.i. Confocal analyses using ZIKV NS2b protein staining confirmed productive infection of LN macrophages in the PLN and ILN of CD169 cKO mice (Figures 4B and 4C). These data indicate that CD169$^+$ macrophages, including those in the LNs, serve as targets for early ZIKV replication.

Dermal dendritic cell migration is not required for viral transit to the blood after footpad inoculation

Although dermal DCs are thought to carry infectious virus to the LNs to initiate nodal infection and adaptive immune responses, our kinetic examination of nodal macrophage infection suggested that macrophages were infected before DC trafficking from the skin, which takes at least 6 h to occur.[47] Therefore, we next quantitated virus at the inoculation site (foot), LNs, and serum of CD169 cKO mice at 12 h p.i. (Figure 5A). Although we detected viral dissemination in the serum by 12 h in *Ifnar1*$^{-/-}$ and CD169 cKO mice, we did not yet detect infectious virus in foot homogenates (Figure 5A). Viral titers were statistically similar between *Ifnar1*$^{-/-}$ and CD169 cKO mice at this early time point.

Skin-resident dermal DCs and Langerhans cells use the chemokine receptor CCR7 to migrate via the lymphatics to the skin-draining LN.[48] To dissect the contribution of DC/Langerhans cell migration from the skin to LN infection, we treated *Ccr7*$^{-/-}$ mice (lacking DC lymphatic migration; Figure S3) with an anti-IFNAR1 Ab and quantitated infectious virus at 24 h p.i. (Figure 5B). Viral titers in the PLN were not statistically different regardless of DC migration, and mice still developed similar levels of viremia.

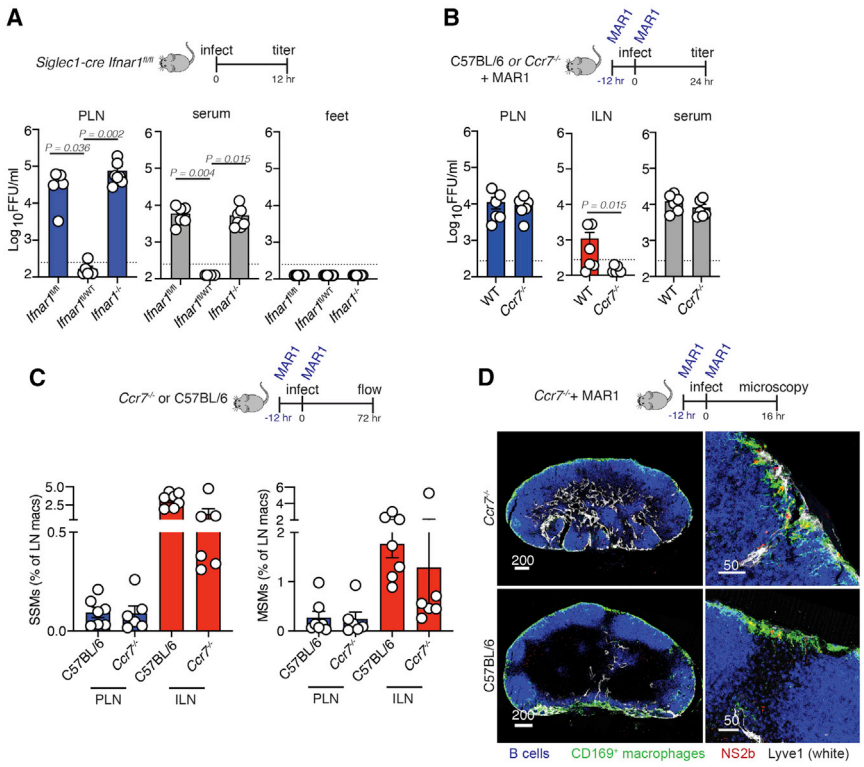

Figure 5. Migrating dendritic cells are dispensable for ZIKV dissemination after FP inoculation

(A) Viral titers (FFUs per milliliter) in the PLN (left, blue bars), serum (center, gray bars), and FP (right, yellow bars) harvested 12 h p.i. from *Siglec1-cre Ifnar*$^{fl/fl}$ (homozygous *Ifnar1* knockout in CD169^{+} cells [cKO]) mice, *Siglec1-cre Ifnar*$^{fl/WT}$ (heterozygous cKO) mice, and *Ifnar1*$^{-/-}$ mice inoculated with 10^4 FFUs of ZIKV. The experiment was repeated 2 times with 3 mice per group. Results shown are pooled from two independent experiments. Dots represent individual mice (either pooled LNs or separate serum or feet) and the average of technical replicates. Dashed line, LOD for the assay. Values below the LOD are reported as half the LOD (125 FFU/mL).

(B) Viral titers (FFUs per milliliter) in the PLN (left, blue bars), ILN (center, red bars), and serum (right, gray bars) harvested 12 h p.i. from C57BL/6 or *Ccr7*$^{-/-}$ mice treated with the anti-IFNAR1 Ab MAR1-5A3 and inoculated with 10^4 FFUs of ZIKV. The experiment was repeated 2 times with 3 mice per group. Results shown are pooled from two independent experiments. Dots represent individual mice (either pooled LNs or separate serum) and the average of technical replicates. Dashed line, LOD for the assay. Values below the LOD are reported as half the LOD (125 FFU/mL).

(C) Frequency of CD169^{+} SSMs (left) and MSMs (right) in the either PLNs (blue bars) or ILNs (red bars) 72 h p.i. of C57BL/6 or *Ccr7*$^{-/-}$ mice as a percentage of total LN macrophages Statistics, one-way ANOVA. Dots show pooled LNs from individual mice. Error bars, SEM. The experiment was repeated 2 times with 3 mice/group.

(D) Confocal images of frozen LN sections from nodes harvested 16 h p.i. from C57BL/6 or *Ccr7*$^{-/-}$ mice treated with an anti-IFNAR1 Ab. Blue, B cells; green, CD169^{+} macrophages; red, ZIKV NS2b; white, Lyve1. Right panels show a higher magnification of infected SSMs. Scale bars are in micrometers.

Notably, CCR7 deficiency significantly decreased viral titers in the ILN, suggesting that cellular movement either from or within the PLN impacts viral transport to downstream LNs. Flow cytometry at 72 h revealed attrition of SSMs and MSMs in the PLN and ILN (Figure 5C), indicating that DC migration is not required for disruption of nodal macrophage networks. We confirmed productive infection of LN macrophages in anti-IFNAR1 Ab-treated *Ccr7*$^{-/-}$ mice through confocal microscopy and staining for NS2b (Figure 5D). Thus, our data suggest that macrophages can produce the virus needed for early systemic dissemination in the absence of a significant contribution of infectious virus from migratory DCs.

Infected monocytes do not account for high levels of virus in the blood

Monocytes are mobile myeloid cells rapidly recruited to sites of infection, where they typically die or mature into sedentary tissue macrophages.[49] Flavivirus infection of mice and humans results in monocyte mobilization from the bone marrow into the blood and then the skin, where they are thought to serve as targets of infection.[20,21,28] Furthermore, monocytes have been proposed to become "Trojan horses" for ZIKV and act as a major cell population disseminating the virus in mice.[23] Based on these studies, we assessed the role of Ly6c^{high} monocytes during early ZIKV dissemination (Figures 6A and 6B). ZIKV infection mobilized monocytes into the blood within 24 h of infection. (Figure 6B, left). Although monocytes were detected in the infected PLN, treatment with an anti-IFNAR1 Ab greatly reduced monocyte nodal numbers (Figure 6B, right). To deplete monocytes, we treated mice with the depleting monoclonal Ab (mAb) GR1 (against Ly6C and Ly6G) as described previously[50] (Figure S4). GR1 treatment eliminated most Ly6C^{high} monocytes and neutrophils in the blood and PLN before and after infection.

Using confocal and multiphoton microscopy, we examined PLN sections (either live or frozen fixed) for the presence of monocytes in LysM-eGFP reporter mice, which possess green myelomonocytes of varying GFP intensity (neutrophils [bright], monocytes [bright intermediate], and macrophages [dim]).[51] Whereas eGFP-bright neutrophils accumulated in and near the SCS around ZIKV-infected and dying macrophages, we did not detect NS2b-expressing eGFP^{+} cells at the time points examined (8–24 h p.i.) (Figures 6C and S4). Furthermore, depletion of monocytes did not impact infectious viral titers in the PLN or serum at 24 h p.i. (Figure 6D).

Collectively, these data indicate that Ly6C^{high} monocytes are not trafficking infectious virus from the skin into the LNs or blood early during infection. Furthermore, infection of blood monocytes is not required for the high levels of blood-borne ZIKV in these mouse models.

CD169^{+} macrophage infection alone does not induce systemic disease

We next examined the contribution of CD169^{+} macrophage infection to the sustained viremia detected in *Ifnar1*$^{-/-}$ mice

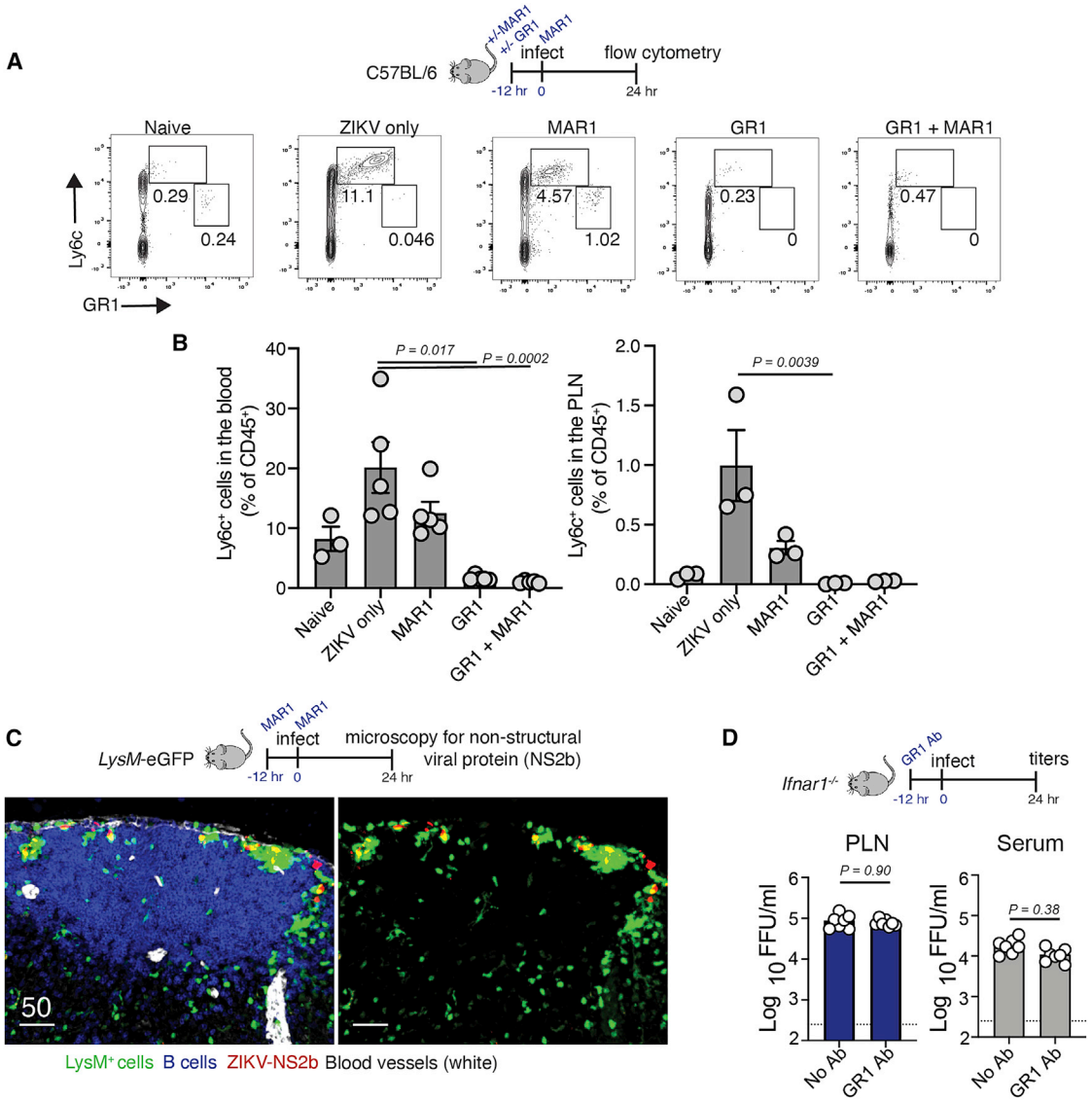

Figure 6. Monocytes are not needed for early ZIKV dissemination

(A) Flow cytometry plots generated from single-cell suspensions of PLNs harvested from naive C57BL/6 mice (left) and infected C57BL/6 mice at 24 h p.i. (all other panels). Where indicated, mice were given the MAR1-5A3 (anti-IFNAR1) or GR1 Ab before infection. An additional dose of MAR1-5A3 was given at the time of infection. Cells were first gated on $CD45^+$ cells. Gating indicates $Ly6C^+$ monocytes (top boxes) and $Ly6G^+$ neutrophils (center boxes).

(B) Frequency of $Ly6C^+$ monocytes in the blood (left) and PLN (right) of the indicated mice 24 h p.i. Statistics, one-way ANOVA. Dots show pooled LNs from individual mice. Error bars, SEM. The experiment was repeated 2 times with 3–5 mice/group.

(C) Confocal images of frozen PLN sections from nodes harvested 24 h p.i. from LysM-eGFP mice treated with MAR1-5A3. B220, blue; LysM-eGFP$^+$ cells, green; blood vessel (CD31), white; ZIKV NS2b protein, red. The right panels omit B cells for clarity. Scale bars are in micrometers.

(D) Viral titers (FFUs per milliliter) in the PLN (left, blue bars) and serum (right, gray bars) harvested 24 h p.i. from *Ifnar1*$^{-/-}$ mice inoculated with 10^4 FFUs of ZIKV. Mice were given the GR1 Ab prior to infection. The experiment was repeated 3 times with 3–4 mice per group. Dots represent individual mice (either pooled LNs or separate serum) and the average of technical replicates. Dashed line, LOD for the assay. Statistics, unpaired t test.

through 5 days p.i. (Figure 7A). Notably, viral titers in the serum were low in CD169 cKO mice on day 3 p.i., and little infectious ZIKV was present in the serum on day 5 p.i. (Figure 7B). Similarly, viral titers in the PLN were low in CD169 cKO mice on day 3 p.i., but not in *Ifnar1*$^{-/-}$ mice, suggesting that there are additional targets for ZIKV infection in the LNs leading to sustained viral production. Consistent with reduced nodal and serum viral levels, CD169 cKO mice exhibited no weight loss or mortality after inoculation with the same dose of virus that resulted in marked virus-induced morbidity in *Ifnar1*$^{-/-}$ mice (Figure 7C). Collectively, our data indicate that nodal macrophages contribute to viral dissemination from the LNs; however, infection of other cells is needed for virus-induced morbidity.

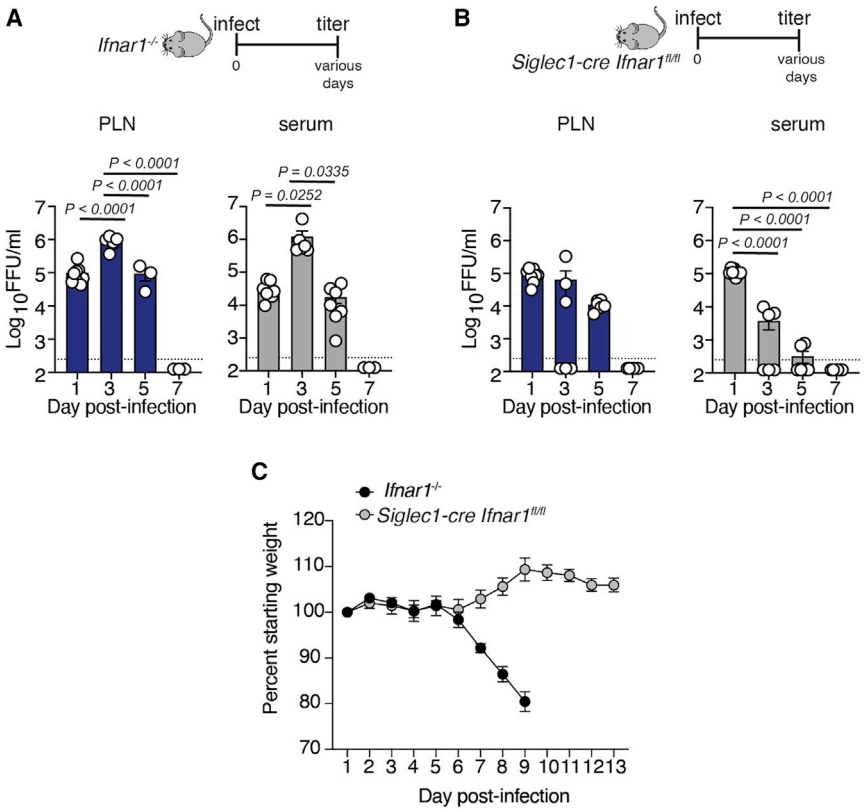

Figure 7. CD169⁺ macrophage infection does not result in morbidity

(A) Viral titers (FFUs per milliliter) in the PLN (left, blue dots) and serum (right, gray bars) harvested at the indicated day p.i. from *Ifnar1*$^{-/-}$ mice. The experiment was repeated 2 times with 3–4 mice per group. Results shown are pooled from two experiments. Dots represent individual mice (either pooled LNs or separate serum) and the average of technical replicates. Dashed line, LOD for the assay. Values below the LOD are reported as half the LOD (125 FFU/mL).

(B) As in (A) but in *Siglec1-cre Ifnar*$^{fl/fl}$ (cKO) mice.

(C) Weight loss (as a percentage of starting weight) in *Ifnar1*$^{-/-}$ and *Siglec1-cre Ifnar*$^{fl/fl}$ (cKO) mice. Dots show average weight per day p.i. (indicated on the x axis). The experiment was repeated twice with 4–5 mice/group. Scale bars, SEM. Statistics, one-way ANOVA.

DISCUSSION

Many medically important viral pathogens, including ZIKV and monkeypox virus, follow a similar initial distribution route through the host during infection. After viral entry via a breach in an epithelial barrier, virus travels to and replicates in the draining LN. After the LN, virus can be detected in the blood and eventually in distal tissues, where the consequences of viral infection are often observable as host pathology. Each step in this process involves movement of the virus into a new part of the body against physical and immunological barriers. For example, upon tissue entry, phagocytes of the innate immune system can capture the virus to eliminate spread and produce cytokines that limit viral replication in the tissue.[52] When the virus reaches the blood, endothelial cells form a primary barrier preventing diffusion of the virus into the tissue.[53] While mechanisms enabling viral circumvention of some of these important controls of systemic homeostasis are well established, our knowledge of events unfolding in some areas, such as the LNs, is still limited.

One strategy allowing a virus to bypass normal barriers against spread is to transit with immune cells that migrate throughout the body. The number of migratory immune cells, particularly blood monocytes, increases by orders of magnitude during infection. Numerous studies in mice and humans have identified ZIKV-infected monocytes in the blood or in peripheral organs.[20–23,25] The results of these studies, along with others during infections with related flaviviruses, have led to the idea that myeloid cells are critical for viral dissemination from the skin. However, monocytes could function to spread the virus at multiple time points during infection. Our studies refine the events leading to ZIKV in the tissues to include LN macrophages as cells that are responsible for the initial movement from the LNs. Monocyte involvement likely occurs as ZIKV spreads from the blood to distal tissues. Depletion of monocytes did not impact early viral burden in the serum, suggesting that monocytes are not the source of early virus in the blood. Monocyte infection could occur as a result of viremia and might be enhanced by the increased monocyte mobilization seen during infection.

In addition to monocytes, migratory dermal DCs are implicated in the spread of ZIKV and other flaviviruses from the skin.[23,27,30,54–60] Given the right stimulation, DCs clearly possess the capacity to migrate from virally infected tissues to the LNs.[48] To our knowledge, however, ZIKV-infected migratory DCs have not been isolated from or identified in the LNs. In a previous study, we microscopically examined ZIKV-infected LNs 24 h after infection and did not identify infected migratory DCs.[39] Our data here indicate that ZIKV is present in the blood before large numbers of DCs migrate into the LNs. Future experiments will be required to understand the role of infected DCs at later time points in the pathogenesis sequence. Recent studies with the poxvirus vaccinia virus have demonstrated that the immune system can halt viral spread after cutaneous viral replication by shutting off lymphatic transport of the virus or by preventing DC trafficking to the LNs.[61,62] If these skin immune-defense mechanisms also occur during ZIKV infection, then viral replication in the skin might not directly translate to infectious virus in the blood. Nonetheless, local viral replication in the skin is poised to influence viremia through indirect mechanisms, such as pro-inflammatory cytokine production.

The lymphatics can deliver a first bolus of virus to the LNs for capture by strategically positioned macrophages and DCs.[39,63,64] This early virus delivery initiates the adaptive immune

response by providing antigen for B cell activation and allowing priming of $CD8^+$ T cells by LN-resident DCs.[39,64,65] However, given the small number of SSMs in the LNs (with some estimates of only 200 SSMs per PLN[43]), we evaluated whether LN macrophages could produce sufficient virus for downstream infection. Our data in CD169 cKO mice suggest that this small group of LN cells can produce enough virus to result in detectable viremia by 12 h p.i. Future studies will be needed to determine the sources for continued virus output in CD169 cKO mice (for example, other LNs in the chain or $CD169^+$ macrophages in other tissues, such as the spleen). Although high levels of blood-borne virus could be detected in *Ifnar1*$^{-/-}$ animals 5 days p.i., viremia waned in CD169 cKO mice. This result suggests that there is a finite population of $CD169^+$ macrophages that can produce ZIKV.

SSMs undergo attrition during LN infection, vaccination, and inflammation.[41] The mechanisms leading to SSM death have been debated (e.g., pyroptosis versus necroptosis)[41–43] because SSMs that are not directly infected also die after stimulation. This observation is perplexing because LN macrophage death impairs LN filtration as well as development of humoral immune responses to secondary pathogens. Based on our data, we propose that LN macrophage death represents a programmed response to limit virus production by eliminating uninfected cells that could serve as vessels to amplify and disseminate the virus.

Collectively, our data reveal that lymphatics and LN sinusoidal macrophages are key participants in dissemination of ZIKV to and from the LNs. Early viral spread to the blood occurred in the absence of cellular transport by DCs or monocytes. Together, our data illuminate a time point during ZIKV dissemination that could be targeted to prevent downstream infection before viral movement into peripheral tissues.

Limitations of the study

Our studies used murine models of ZIKV infection where the virus was delivered by an injection. This route of inoculation likely differs from human infection after a mosquito bite in terms of cell types infected and the kinetics of infection. The volume of inoculation also differs from that delivered by a mosquito and may particularly affect the requirement for different cell types to carry the virus to the LNs from the skin. Future studies will be needed to determine whether migratory DCs are required for early ZIKV dissemination after a mosquito bite but not footpad inoculation. Additionally, mosquito saliva has immunomodulatory effects that are not accounted for in our models.[56,66,67]

STAR★METHODS

Detailed methods are provided in the online version of this paper and include the following:

SUPPLEMENTAL INFORMATION

Supplemental information can be found online at https://doi.org/10.1016/j.celrep.2023.112126.

ACKNOWLEDGMENTS

This work was supported by the Intramural Research Program of the NIAID and NIH (R01AI073755 to M.S.D.). The graphical abstract was drawn by Ethan Tyler (NIH Medical Arts Branch).

AUTHOR CONTRIBUTIONS

Conceptualization, H.D.H.; methodology, H.D.H., G.V.R., D.N.G., and T.C.P.; materials, M.S.D., K.A., and Y.A.; investigation, G.V.R., D.N.G., A.K., C.C.A., M.A., J.P.S., S.M.V., C.R.C., C.S.M., A.C.H., K.A.D., S.M., and H.D.H.; writing – original draft, H.D.H.; writing – review and editing, all authors; supervision, H.D.H., T.C.P., and M.S.D.; funding acquisition, H.D.H., T.C.P., and M.S.D.

DECLARATION OF INTERESTS

M.S.D. is a consultant for Inbios, Vir Biotechnology, Senda Biosciences, Moderna, and Immunome. The Diamond laboratory has received unrelated funding support in sponsored research agreements from Vir Biotechnology, Emergent BioSolutions, Generate Biomedicines, and Moderna.

Received: September 21, 2022
Revised: January 3, 2023
Accepted: February 1, 2023
Published: February 15, 2023

REFERENCES

1. Pierson, T.C., and Diamond, M.S. (2020). The continued threat of emerging flaviviruses. Nat. Microbiol. *5*, 796–812. https://doi.org/10.1038/s41564-020-0714-0.
2. Diamond, M.S., Ledgerwood, J.E., and Pierson, T.C. (2019). Zika virus vaccine development: progress in the face of new challenges. Annu. Rev. Med. *70*, 121–135. https://doi.org/10.1146/annurev-med-040717-051127.
3. Paz-Bailey, G., Rosenberg, E.S., Doyle, K., Munoz-Jordan, J., Santiago, G.A., Klein, L., Perez-Padilla, J., Medina, F.A., Waterman, S.H., Gubern, C.G., et al. (2018). Persistence of Zika virus in body fluids - final report. N. Engl. J. Med. *379*, 1234–1243. https://doi.org/10.1056/NEJMoa1613108.
4. Mlakar, J., Korva, M., Tul, N., Popović, M., Poljšak-Prijatelj, M., Mraz, J., Kolenc, M., Resman Rus, K., Vesnaver Vipotnik, T., Fabjan Vodušek, V., et al. (2016). Zika virus associated with microcephaly. N. Engl. J. Med. *374*, 951–958. https://doi.org/10.1056/NEJMoa1600651.
5. Shan, C., Xie, X., and Shi, P.Y. (2018). Zika virus vaccine: progress and challenges. Cell Host Microbe *24*, 12–17. https://doi.org/10.1016/j.chom.2018.05.021.
6. Dowd, K.A., Ko, S.Y., Morabito, K.M., Yang, E.S., Pelc, R.S., DeMaso, C.R., Castilho, L.R., Abbink, P., Boyd, M., Nityanandam, R., et al. (2016). Rapid development of a DNA vaccine for Zika virus. Science *354*, 237–240. https://doi.org/10.1126/science.aai9137.

7. Van Rompay, K.K.A., Keesler, R.I., Ardeshir, A., Watanabe, J., Usachenko, J., Singapuri, A., Cruzen, C., Bliss-Moreau, E., Murphy, A.M., Yee, J.L., et al. (2019). DNA vaccination before conception protects Zika virus-exposed pregnant macaques against prolonged viremia and improves fetal outcomes. Sci. Transl. Med. *11*, eaay2736. https://doi.org/10.1126/scitranslmed.aay2736.

8. Abbink, P., Larocca, R.A., Visitsunthorn, K., Boyd, M., De La Barrera, R.A., Gromowski, G.D., Kirilova, M., Peterson, R., Li, Z., Nanayakkara, O., et al. (2017). Durability and correlates of vaccine protection against Zika virus in rhesus monkeys. Sci. Transl. Med. *9*, eaao4163. https://doi.org/10.1126/scitranslmed.aao4163.

9. Richner, J.M., Himansu, S., Dowd, K.A., Butler, S.L., Salazar, V., Fox, J.M., Julander, J.G., Tang, W.W., Shresta, S., Pierson, T.C., et al. (2017). Modified mRNA vaccines protect against Zika virus infection. Cell *168*, 1114–1125.e10. https://doi.org/10.1016/j.cell.2017.02.017.

10. Gorman, M.J., Caine, E.A., Zaitsev, K., Begley, M.C., Weger-Lucarelli, J., Uccellini, M.B., Tripathi, S., Morrison, J., Yount, B.L., Dinnon, K.H., 3rd., et al. (2018). An immunocompetent mouse model of Zika virus infection. Cell Host Microbe *23*, 672–685.e6. https://doi.org/10.1016/j.chom.2018.04.003.

11. Lazear, H.M., Govero, J., Smith, A.M., Platt, D.J., Fernandez, E., Miner, J.J., and Diamond, M.S. (2016). A mouse model of Zika virus pathogenesis. Cell Host Microbe *19*, 720–730. https://doi.org/10.1016/j.chom.2016.03.010.

12. Morrison, T.E., and Diamond, M.S. (2017). Animal models of Zika virus infection, pathogenesis, and immunity. J. Virol. *91*, e00009-17. https://doi.org/10.1128/JVI.00009-17.

13. Yockey, L.J., Jurado, K.A., Arora, N., Millet, A., Rakib, T., Milano, K.M., Hastings, A.K., Fikrig, E., Kong, Y., Horvath, T.L., et al. (2018). Type I interferons instigate fetal demise after Zika virus infection. Sci. Immunol. *3*, eaao1680. https://doi.org/10.1126/sciimmunol.aao1680.

14. Miner, J.J., Cao, B., Govero, J., Smith, A.M., Fernandez, E., Cabrera, O.H., Garber, C., Noll, M., Klein, R.S., Noguchi, K.K., et al. (2016). Zika virus infection during pregnancy in mice causes placental damage and fetal demise. Cell *165*, 1081–1091. https://doi.org/10.1016/j.cell.2016.05.008.

15. Liu, S., DeLalio, L.J., Isakson, B.E., and Wang, T.T. (2016). AXL-mediated productive infection of human endothelial cells by Zika virus. Circ. Res. *119*, 1183–1189. https://doi.org/10.1161/circresaha.116.309866.

16. Richard, A.S., Shim, B.S., Kwon, Y.C., Zhang, R., Otsuka, Y., Schmitt, K., Berri, F., Diamond, M.S., and Choe, H. (2017). AXL-dependent infection of human fetal endothelial cells distinguishes Zika virus from other pathogenic flaviviruses. Proc. Natl. Acad. Sci. USA *114*, 2024–2029. https://doi.org/10.1073/pnas.1620558114.

17. Mladinich, M.C., Schwedes, J., and Mackow, E.R. (2017). Zika virus persistently infects and is basolaterally released from primary human brain microvascular endothelial cells. mBio *8*, e00952-17. https://doi.org/10.1128/mBio.00952-17.

18. Lemke, G. (2013). Biology of the TAM receptors. Cold Spring Harb. Perspect. Biol. *5*, a009076. https://doi.org/10.1101/cshperspect.a009076.

19. Hastings, A.K., Yockey, L.J., Jagger, B.W., Hwang, J., Uraki, R., Gaitsch, H.F., Parnell, L.A., Cao, B., Mysorekar, I.U., Rothlin, C.V., et al. (2017). TAM receptors are not required for Zika virus infection in mice. Cell Rep. *19*, 558–568. https://doi.org/10.1016/j.celrep.2017.03.058.

20. Michlmayr, D., Andrade, P., Gonzalez, K., Balmaseda, A., and Harris, E. (2017). CD14(+)CD16(+) monocytes are the main target of Zika virus infection in peripheral blood mononuclear cells in a paediatric study in Nicaragua. Nat. Microbiol. *2*, 1462–1470. https://doi.org/10.1038/s41564-017-0035-0.

21. Foo, S.S., Chen, W., Chan, Y., Bowman, J.W., Chang, L.C., Choi, Y., Yoo, J.S., Ge, J., Cheng, G., Bonnin, A., et al. (2017). Asian Zika virus strains target CD14(+) blood monocytes and induce M2-skewed immunosuppression during pregnancy. Nat. Microbiol. *2*, 1558–1570. https://doi.org/10.1038/s41564-017-0016-3.

22. Ayala-Nunez, N.V., Follain, G., Delalande, F., Hirschler, A., Partiot, E., Hale, G.L., Bollweg, B.C., Roels, J., Chazal, M., Bakoa, F., et al. (2019). Zika virus enhances monocyte adhesion and transmigration favoring viral dissemination to neural cells. Nat. Commun. *10*, 4430. https://doi.org/10.1038/s41467-019-12408-x.

23. McDonald, E.M., Anderson, J., Wilusz, J., Ebel, G.D., and Brault, A.C. (2020). Zika virus replication in myeloid cells during acute infection is vital to viral dissemination and pathogenesis in a mouse model. J. Virol. *94*, e00838-20. https://doi.org/10.1128/JVI.00838-20.

24. Teh, Y.C., Ding, J.L., Ng, L.G., and Chong, S.Z. (2019). Capturing the fantastic voyage of monocytes through time and space. Front. Immunol. *10*, 834. https://doi.org/10.3389/fimmu.2019.00834.

25. Jurado, K.A., and Iwasaki, A. (2017). Zika virus targets blood monocytes. Nat. Microbiol. *2*, 1460–1461. https://doi.org/10.1038/s41564-017-0049-7.

26. Cerny, D., Haniffa, M., Shin, A., Bigliardi, P., Tan, B.K., Lee, B., Poidinger, M., Tan, E.Y., Ginhoux, F., and Fink, K. (2014). Selective susceptibility of human skin antigen presenting cells to productive dengue virus infection. PLoS Pathog. *10*, e1004548. https://doi.org/10.1371/journal.ppat.1004548.

27. Duangkhae, P., Erdos, G., Ryman, K.D., Watkins, S.C., Falo, L.D., Jr., Marques, E.T.A., Jr., and Barratt-Boyes, S.M. (2018). Interplay between keratinocytes and myeloid cells drives dengue virus spread in human skin. J. Invest. Dermatol. *138*, 618–626. https://doi.org/10.1016/j.jid.2017.10.018.

28. Schmid, M.A., and Harris, E. (2014). Monocyte recruitment to the dermis and differentiation to dendritic cells increases the targets for dengue virus replication. PLoS Pathog. *10*, e1004541. https://doi.org/10.1371/journal.ppat.1004541.

29. Wu, S.J., Grouard-Vogel, G., Sun, W., Mascola, J.R., Brachtel, E., Putvatana, R., Louder, M.K., Filgueira, L., Marovich, M.A., Wong, H.K., et al. (2000). Human skin Langerhans cells are targets of dengue virus infection. Nat. Med. *6*, 816–820. https://doi.org/10.1038/77553.

30. Hamel, R., Dejarnac, O., Wichit, S., Ekchariyawat, P., Neyret, A., Luplertlop, N., Perera-Lecoin, M., Surasombatpattana, P., Talignani, L., Thomas, F., et al. (2015). Biology of Zika virus infection in human skin cells. J. Virol. *89*, 8880–8896. https://doi.org/10.1128/JVI.00354-15.

31. Grant, A., Ponia, S.S., Tripathi, S., Balasubramaniam, V., Miorin, L., Sourisseau, M., Schwarz, M.C., Sánchez-Seco, M.P., Evans, M.J., Best, S.M., and García-Sastre, A. (2016). Zika virus targets human STAT2 to inhibit type I interferon signaling. Cell Host Microbe *19*, 882–890. https://doi.org/10.1016/j.chom.2016.05.009.

32. Ozawa, M., Nakajima, S., Kobayashi, D., Tomii, K., Li, N.J., Watarai, T., Suzuki, R., Watanabe, S., Kanda, Y., Takeuchi, A., and Katakai, T. (2022). Micro- and macro-anatomical frameworks of lymph nodes indispensable for the lymphatic system filtering function. Front. Cell Dev. Biol. *10*, 902601. https://doi.org/10.3389/fcell.2022.902601.

33. Harrell, M.I., Iritani, B.M., and Ruddell, A. (2008). Lymph node mapping in the mouse. J. Immunol. Methods *332*, 170–174. https://doi.org/10.1016/j.jim.2007.11.012.

34. Bellomo, A., Gentek, R., Bajénoff, M., and Baratin, M. (2018). Lymph node macrophages: scavengers, immune sentinels and trophic effectors. Cell. Immunol. *330*, 168–174. https://doi.org/10.1016/j.cellimm.2018.01.010.

35. Gray, E.E., and Cyster, J.G. (2012). Lymph node macrophages. J. Innate Immun. *4*, 424–436. https://doi.org/10.1159/000337007.

36. Mondor, I., Baratin, M., Lagueyrie, M., Saro, L., Henri, S., Gentek, R., Suerinck, D., Kastenmuller, W., Jiang, J.X., and Bajénoff, M. (2019). Lymphatic endothelial cells are essential components of the subcapsular sinus macrophage niche. Immunity *50*, 1453–1466.e4. https://doi.org/10.1016/j.immuni.2019.04.002.

37. Phan, T.G., Green, J.A., Gray, E.E., Xu, Y., and Cyster, J.G. (2009). Immune complex relay by subcapsular sinus macrophages and noncognate B cells drives antibody affinity maturation. Nat. Immunol. *10*, 786–793. https://doi.org/10.1038/ni.1745.

38. Jafarnejad, M., Woodruff, M.C., Zawieja, D.C., Carroll, M.C., and Moore, J.E., Jr. (2015). Modeling lymph flow and fluid exchange with blood vessels in lymph nodes. Lymphat. Res. Biol. *13*, 234–247. https://doi.org/10.1089/lrb.2015.0028.

39. Reynoso, G.V., Weisberg, A.S., Shannon, J.P., McManus, D.T., Shores, L., Americo, J.L., Stan, R.V., Yewdell, J.W., and Hickman, H.D. (2019). Lymph node conduits transport virions for rapid T cell activation. Nat. Immunol. *20*, 602–612. https://doi.org/10.1038/s41590-019-0342-0.

40. Sung, J.H., Zhang, H., Moseman, E.A., Alvarez, D., Iannacone, M., Henrickson, S.E., de la Torre, J.C., Groom, J.R., Luster, A.D., and von Andrian, U.H. (2012). Chemokine guidance of central memory T cells is critical for antiviral recall responses in lymph nodes. Cell *150*, 1249–1263. https://doi.org/10.1016/j.cell.2012.08.015.

41. Gaya, M., Castello, A., Montaner, B., Rogers, N., Reis e Sousa, C., Bruckbauer, A., and Batista, F.D. (2015). Host response. Inflammation-induced disruption of SCS macrophages impairs B cell responses to secondary infection. Science *347*, 667–672. https://doi.org/10.1126/science.aaa1300.

42. Sagoo, P., Garcia, Z., Breart, B., Lemaître, F., Michonneau, D., Albert, M.L., Levy, Y., and Bousso, P. (2016). In vivo imaging of inflammasome activation reveals a subcapsular macrophage burst response that mobilizes innate and adaptive immunity. Nat. Med. *22*, 64–71. https://doi.org/10.1038/nm.4016.

43. Chatziandreou, N., Farsakoglu, Y., Palomino-Segura, M., D'Antuono, R., Pizzagalli, D.U., Sallusto, F., Lukacs-Kornek, V., Uguccioni, M., Corti, D., Turley, S.J., et al. (2017). Macrophage death following influenza vaccination initiates the inflammatory response that promotes dendritic cell function in the draining lymph node. Cell Rep. *18*, 2427–2440. https://doi.org/10.1016/j.celrep.2017.02.026.

44. Gray, E.E., Friend, S., Suzuki, K., Phan, T.G., and Cyster, J.G. (2012). Subcapsular sinus macrophage fragmentation and CD169+ bleb acquisition by closely associated IL-17-committed innate-like lymphocytes. PLoS One *7*, e38258. https://doi.org/10.1371/journal.pone.0038258.

45. Karasawa, K., Asano, K., Moriyama, S., Ushiki, M., Monya, M., Iida, M., Kuboki, E., Yagita, H., Uchida, K., Nitta, K., and Tanaka, M. (2015). Vascular-resident CD169-positive monocytes and macrophages control neutrophil accumulation in the kidney with ischemia-reperfusion injury. J. Am. Soc. Nephrol. *26*, 896–906. https://doi.org/10.1681/ASN.2014020195.

46. Prigge, J.R., Hoyt, T.R., Dobrinen, E., Capecchi, M.R., Schmidt, E.E., and Meissner, N. (2015). Type I IFNs act upon hematopoietic progenitors to protect and maintain hematopoiesis during pneumocystis lung infection in mice. J. Immunol. *195*, 5347–5357. https://doi.org/10.4049/jimmunol.1501553.

47. Tomura, M., Hata, A., Matsuoka, S., Shand, F.H.W., Nakanishi, Y., Ikebuchi, R., Ueha, S., Tsutsui, H., Inaba, K., Matsushima, K., et al. (2014). Tracking and quantification of dendritic cell migration and antigen trafficking between the skin and lymph nodes. Sci. Rep. *4*, 6030. https://doi.org/10.1038/srep06030.

48. Platt, A.M., and Randolph, G.J. (2013). Dendritic cell migration through the lymphatic vasculature to lymph nodes. Adv. Immunol. *120*, 51–68. https://doi.org/10.1016/B978-0-12-417028-5.00002-8.

49. Italiani, P., and Boraschi, D. (2014). From monocytes to M1/M2 macrophages: phenotypical vs. Functional differentiation. Front. Immunol. *5*, 514. https://doi.org/10.3389/fimmu.2014.00514.

50. Hickman, H.D., Reynoso, G.V., Ngudiankama, B.F., Rubin, E.J., Magadán, J.G., Cush, S.S., Gibbs, J., Molon, B., Bronte, V., Bennink, J.R., and Yewdell, J.W. (2013). Anatomically restricted synergistic antiviral activities of innate and adaptive immune cells in the skin. Cell Host Microbe *13*, 155–168. https://doi.org/10.1016/j.chom.2013.01.004.

51. Faust, N., Varas, F., Kelly, L.M., Heck, S., and Graf, T. (2000). Insertion of enhanced green fluorescent protein into the lysozyme gene creates mice with green fluorescent granulocytes and macrophages. Blood *96*, 719–726.

52. Shi, C., and Pamer, E.G. (2011). Monocyte recruitment during infection and inflammation. Nat. Rev. Immunol. *11*, 762–774. https://doi.org/10.1038/nri3070.

53. Mehta, D., and Malik, A.B. (2006). Signaling mechanisms regulating endothelial permeability. Physiol. Rev. *86*, 279–367. https://doi.org/10.1152/physrev.00012.2005.

54. Lei, V., Petty, A.J., Atwater, A.R., Wolfe, S.A., and MacLeod, A.S. (2020). Skin viral infections: host antiviral innate immunity and viral immune evasion. Front. Immunol. *11*, 593901. https://doi.org/10.3389/fimmu.2020.593901.

55. King, C.A., Wegman, A.D., and Endy, T.P. (2020). Mobilization and activation of the innate immune response to dengue virus. Front. Cell. Infect. Microbiol. *10*, 574417. https://doi.org/10.3389/fcimb.2020.574417.

56. Schneider, C.A., Calvo, E., and Peterson, K.E. (2021). Arboviruses: how saliva impacts the journey from vector to host. Int. J. Mol. Sci. *22*, 9173. https://doi.org/10.3390/ijms22179173.

57. Castillo, J.A., Naranjo, J.S., Rojas, M., Castaño, D., and Velilla, P.A. (2019). Role of monocytes in the pathogenesis of dengue. Arch. Immunol. Ther. Exp. *67*, 27–40. https://doi.org/10.1007/s00005-018-0525-7.

58. Troupin, A., Shirley, D., Londono-Renteria, B., Watson, A.M., McHale, C., Hall, A., Hartstone-Rose, A., Klimstra, W.B., Gomez, G., and Colpitts, T.M. (2016). A role for human skin mast cells in dengue virus infection and systemic spread. J. Immunol. *197*, 4382–4391. https://doi.org/10.4049/jimmunol.1600846.

59. Begum, F., Das, S., Mukherjee, D., Mal, S., and Ray, U. (2019). Insight into the tropism of dengue virus in humans. Viruses *11*, 1136.

60. Rathore, A.P.S., and St John, A.L. (2018). Immune responses to dengue virus in the skin. Open Biol. *8*, 180087. https://doi.org/10.1098/rsob.180087.

61. Aggio, J.B., Krmeská, V., Ferguson, B.J., Wowk, P.F., and Rothfuchs, A.G. (2021). Vaccinia virus infection inhibits skin dendritic cell migration to the draining lymph node. J. Immunol. *206*, 776–784. https://doi.org/10.4049/jimmunol.2000928.

62. Churchill, M.J., du Bois, H., Heim, T.A., Mudianto, T., Steele, M.M., Nolz, J.C., and Lund, A.W. (2022). Infection-induced lymphatic zippering restricts fluid transport and viral dissemination from skin. J. Exp. Med. *219*, e20211830. https://doi.org/10.1084/jem.20211830.

63. Hickman, H.D., Takeda, K., Skon, C.N., Murray, F.R., Hensley, S.E., Loomis, J., Barber, G.N., Bennink, J.R., and Yewdell, J.W. (2008). Direct priming of antiviral CD8+ T cells in the peripheral interfollicular region of lymph nodes. Nat. Immunol. *9*, 155–165. https://doi.org/10.1038/ni1557.

64. Junt, T., Moseman, E.A., Iannacone, M., Massberg, S., Lang, P.A., Boes, M., Fink, K., Henrickson, S.E., Shayakhmetov, D.M., Di Paolo, N.C., et al. (2007). Subcapsular sinus macrophages in lymph nodes clear lymph-borne viruses and present them to antiviral B cells. Nature *450*, 110–114. https://doi.org/10.1038/nature06287.

65. Hickman, H.D., Li, L., Reynoso, G.V., Rubin, E.J., Skon, C.N., Mays, J.W., Gibbs, J., Schwartz, O., Bennink, J.R., and Yewdell, J.W. (2011). Chemokines control naive CD8+ T cell selection of optimal lymph node antigen presenting cells. J. Exp. Med. *208*, 2511–2524. https://doi.org/10.1084/jem.20102545.

66. Pingen, M., Bryden, S.R., Pondeville, E., Schnettler, E., Kohl, A., Merits, A., Fazakerley, J.K., Graham, G.J., and McKimmie, C.S. (2016). Host inflammatory response to mosquito bites enhances the severity of arbovirus infection. Immunity *44*, 1455–1469. https://doi.org/10.1016/j.immuni.2016.06.002.

67. Pingen, M., Schmid, M.A., Harris, E., and McKimmie, C.S. (2017). Mosquito biting modulates skin response to virus infection. Trends Parasitol. *33*, 645–657. https://doi.org/10.1016/j.pt.2017.04.003.

68. Asano, K., Nabeyama, A., Miyake, Y., Qiu, C.H., Kurita, A., Tomura, M., Kanagawa, O., Fujii, S.i., and Tanaka, M. (2011). CD169-positive macrophages dominate antitumor immunity by crosspresenting dead cell-associated antigens. Immunity *34*, 85–95. https://doi.org/10.1016/j.immuni.2010.12.011.

69. Brien, J.D., Lazear, H.M., and Diamond, M.S. (2013). Propagation, quantification, detection, and storage of West Nile virus. Curr.

Protoc. Microbiol. *31*, 15d.13.11–15d.13.18. https://doi.org/10.1002/9780471729259.mc15d03s31.

70. Zhao, H., Fernandez, E., Dowd, K.A., Speer, S.D., Platt, D.J., Gorman, M.J., Govero, J., Nelson, C.A., Pierson, T.C., Diamond, M.S., and Fremont, D.H. (2016). Structural basis of Zika virus-specific antibody protection. Cell *166*, 1016–1027. https://doi.org/10.1016/j.cell.2016.07.020.

71. Sheehan, K.C.F., Lai, K.S., Dunn, G.P., Bruce, A.T., Diamond, M.S., Heutel, J.D., Dungo-Arthur, C., Carrero, J.A., White, J.M., Hertzog, P.J., and Schreiber, R.D. (2006). Blocking monoclonal antibodies specific for mouse IFN-alpha/beta receptor subunit 1 (IFNAR-1) from mice immunized by in vivo hydrodynamic transfection. J. Interferon Cytokine Res. *26*, 804–819. https://doi.org/10.1089/jir.2006.26.804.

STAR★METHODS

KEY RESOURCES TABLE

REAGENT or RESOURCE	SOURCE	IDENTIFIER
Antibodies		
Anti-ZIKV E protein (polyclonal)	GeneTex	Cat# GTX 133314; RRID: AB_2747413
Anti-ZIKV NS2b protein (polyclonal)	GeneTex	GTX133308; RRID:AB_2715494
CD169 (clone 3D6.112)	BioLegend	Cat# 142419; RRID: AB_2566436
B220 (clone RA3-6B2)	Thermo Fisher Scientific	Cat# 48-0452-82; RRID: AB_1548761
CD31 (clone MEC13.3)	BioLegend	Cat# 102516; RRID: AB_2161029
Lyve1 (clone ALY7)	Thermo Fisher Scientific	Cat# 50-0443-82; RRID_0597449
ER-TR7 (rat monoclonal)	Abcam	Cat# ab51824; RRID: AB_881651
SIGNR1 (clone eBio22D1)	Thermo Fisher Scientific	Cat# 14-2093-82; RRID: AB_795885
CD11c (clone N418)	Thermo Fisher Scientific	Cat# 14-0114-85; RRID: AB_467116
Ly6c APC/Cyanine7 (clone HK1.4)	BioLegend	Cat# 128026; RRID:AB_10640120
Gr-1 eFluor 450 (clone RB6-8C5)	Thermo Fisher Scientific	Cat# 48-5931-82; RRID:AB_1548788
CD45 700 (clone 30-F11)	BioLegend	Cat# 103128; RRID: AB_493715
F4/80 PE (clone BM8)	Thermo Fisher Scientific	Cat# 12-4801-82; RRID: AB_465923
CD11b 594 (clone M1/70)	BioLegend	Cat# 101254; RRID: AB_2563231
CD11c PerCP-Cyanine 5.5 (clone N418)	Thermo Fisher Scientific	Cat# 45-0114-82: RRID: AB_925727
CD3 PE/Cyanine 7 (clone 17A2)	BioLegend	Cat#100220; RRID:AB_1732057
B220 PE/Cyanine 7 (clone RA3-6B2)	Thermo Fisher Scientific	Cat# 25-0452-82; RRID:AB_469627
MAR1-5A3	BioXcell	Cat# BE0241; RRID:AB_2687723
GR1	BioXcell	Cat# BE0075; RRID:AB_10312146
Bacterial and virus strains		
Zika virus H/PF/2013	Pierson laboratory	N/A
Zika virus MA-Dakar	Diamond laboratory	N/A
Chemicals, peptides, and recombinant proteins		
Zombie Aqua™ Fixable Viability Kit	BioLegend	Cat# 423102
Spectral DAPI	Perkin Elmer	FP1490
Ghost dye UV450	Tonbo Biosciences	Cat# 13-0868-T500
BSA	Sigma-Aldrich	Cat# A3059-500G
FBS	Hyclone	Cat# SH30070.03
Triton X-	Sigma-Aldrich	Cat# t9284
Paraformaldehyde	Electron Microscopy Sciences	Cat# 15714-S
Sodium (meta)periodate	Sigma-Aldrich	Cat# S1878-500G
Lysine	Sigma-Aldrich	Cat# L5501-100G
2-Methylbutane (Isopentane)	Sigma-Aldrich	Cat# M32631-500ML
Optimal-cutting-temperature (OCT) compound	Electron Microscopy Sciences	Cat# 62550-01
Methyl cellulose	Sigma-Aldrich	Cat# M0512-250G
Gibco™ Opti-MEM™ Reduced Serum Medium, GlutaMAX™ Supplement	Thermo Fisher Scientific	Cat# 51-985-034-500ML
Penicillin-Streptomycin	Thermo Fisher Scientific	Cat# 15070063
Peroxidase AffiniPure Donkey Anti-Mouse IgG(H + L)	Jackson Laboratories	Cat# 715-035-150
TrueBlue™ Horseradish Peroxidase (HRP) substrate,KPL	VWR	Cat# 95059-168

(*Continued on next page*)

Continued

REAGENT or RESOURCE	SOURCE	IDENTIFIER
Critical commercial reagents		
Lysing Matric S (1/8″) metal beads	MP Biomedicals	Cat# 116925100
Experimental models: Cell lines		
Vero	ATCC	Cat# ATCC CRL-1587
Experimental models: Organisms/strains		
Mice		
Mouse: *C57BL/6N*	Taconic	Cat #C57BL/6N
Mouse: *Ifnar1*$^{-/-}$	NIAID Taconic Research Repository	Cat #314
Mouse: *Siglec1*-cre	Riken	RBRC06239
Mouse: B6(Cg)-*Ifnar1*$^{tm1.1Ees}$/J (*Ifnar1*-fl)	Jackson Laboratories	Cat# 028256; RRID: IMSR_JAX:028,256
Mouse: *Siglec1*-cre *Ifnar1*$^{fl/fl}$	Bred in Hickman laboratory	N/A
Mouse: *Ccr7*$^{-/-}$	NIAID Taconic Research Repository	Cat# 8853
Mouse: *hSTAT2-KI*	Jackson Laboratory	Strain #:031,630 RRID:IMSR_JAX:031,630
Software and algorithms		
FlowJo 10	TreeStar	RRID: SCR_008520
Prism 7 and 8	Graphpad	RRID: SCR_002798
Imaris 9.0.0	Bitplane	RRID: SCR_007370

RESOURCE AVAILABILITY

Lead contact

Further information and requests for resources and reagents should be directed to, and will be fulfilled by, the lead contact: Heather Hickman (hhickman@mail.nih.gov).

Materials availability

All materials developed in this study will be available from the lead contact upon reasonable request.

Data and code availability

- This paper does not report original code.
- Unprocessed data underlying the display items in the manuscript, related to the figures, are available from the lead contact upon request.
- Any additional information required to analyze the data reported in this paper is available from the lead contact upon request.

EXPERIMENTAL MODEL AND SUBJECT DETAILS

Mice

Ifnar1$^{-/-}$ (Line 314), *Ccr7*$^{-/-}$ (Line 8453), and LysM-eGFP (Line 342) were obtained from the National Institute of Allergy and Infectious Diseases intramural research repository at Taconic Farms. Wild-type C57BL/6N mice were obtained from Taconic Farms. *Ifnar1*$^{fl/fl}$ mice (B6(Cg)-Ifnar1tm1.1Ees/J; #28256) were obtained from Jackson Laboratories. CD169-cre mice have been previously reported.[68] Embryos were obtained from Riken, rederived and bred in-house to generate CD169-cre *Ifnar1*$^{fl/fl}$ conditional knockout (cKO) mice. *hStat2-KI* mice in a C57BL/6 background have been reported previously and were bred at Washington University School of Medicine.[10] Male and female mice from 6-12 weeks of age were used for experiments. Mice were housed under specific pathogen-free conditions and provided standard rodent chow and sterile water as necessary. All animal studies were approved by and performed in accordance with the Animal Care and Use Committee of the National Institute of Allergy and Infectious Diseases or Washington University School of Medicine.

Viruses

ZIKV strains H/PF2013 and MA-Dakar[10] were used as indicated.

METHOD DETAILS

Viral infections and titers

Mice were anesthetized using isoflurane and infected in both hind footpads with $1x10^4$ FFU ZIKV H/PF/2013 unless otherwise indicated (for some experiments, only one footpad was infected). In Figure 2E, mice were inoculated with $1x10^4$ FFU MA-Dakar.[10] To determine viral titers, LNs or hind feet were collected at various times p.i. and placed in 250 μL of RPMI +2% FBS + HEPES/LN or 500 μL per foot in metal bead lysing matrix tubes (MP Biomedicals). Samples were homogenized using a Fastprep-24 (MP Biomedicals). Alternatively, blood was collected at the indicated time p.i. into serum gel Z/1.1 tubes (Sarstedt) and serum separated by centrifugation. To measure ZIKV-induced morbidity, mice were weighed before infection and daily thereafter, and the percent starting weight was calculated for each mouse.

Infectious virus titers were determined using a focus-forming assay (FFA).[69] Vero cells were seeded at a concentration of 2×10^4 per well in 96-well plates and incubated at 37°C until 90–100% confluency was reached. Confluent monolayers were inoculated in duplicate with LN homogenates or serum and incubated at 37°C for 4 h. Cells then were overlaid with 1% (wt/vol) methylcellulose (Sigma) in Opti-MEM supplemented (Gibco) with 1% Pen-strep (Gibco) and incubated at 37°C. After 48 h, cells were fixed with 4% paraformaldehyde for 30 min at room temperature. Cells were incubated for 2 h with ZV-67 mAb[70] in PBS supplemented with 0.1% saponin and 0.1% BSA. Plates were washed and stained with HRP-conjugated anti-mouse IgG (Jackson laboratories). Virus-infected foci were visualized using TrueBlue peroxidase substrate (KPL) for 20 min and counted by an ImmunoSpot 5.0.37 microanalyzer (CTL).

Antibody treatment

MAR1-5A3 Ab[71] was administered intraperitoneally at 1 mg in 1 mL of sterile PBS 12 h before and the day of footpad infection. For inflammatory monocyte depletion, GR1 Ab was administered intraperitoneally at 0.25 mg in 1 mL of PBS 12–24 h before infection.

Flow cytometric analyses after enzymatic tissue dissociation

LNs were collected at various times p.i. and single-cell suspensions prepared by digestion with Liberase (Roche) + DNAse (Worthington) for ~1 h at 37°C. Cells were disrupted by 3 rounds of vigorous pipetting, suspensions were filtered through 60 μm nylon-filter capped FACS tubes. LN cells were stained for 20 min on ice with CD45 (clone 30-F11), CD3 (clone 17A2), B220 (clone RA3-6B2), CD11c (clone N418), CD11b (clone M1/70, BioLegend), CD169 (clone 3D6.112), F4/80 (clone BM8), Gr-1(clone RB6-8C5) and/or (HK1.4) and fixable viability dye Ghost Dye UV450 or Zombie Aqua. Samples were washed twice post-staining in Hanks Balanced Salt Solution +0.1% BSA and fixed for 20 min with 3.2% paraformaldehyde. Samples were washed twice in PBS and acquired on a Fortessa flow cytometer (BD Biosciences). Flow data were analyzed using FlowJo Software (TreeStar).

Confocal microscopy of frozen LN sections

LNs were removed at the indicated time p.i., fixed in periodate-lysine-paraformaldehyde (PLP) for 48 h, and moved to 30% sucrose/PBS solution for 24 h. Tissues were embedded in optimal-cutting-temperature (OCT) medium (Electron Microscopy Sciences), oriented to cut through both the B cell follicles and the medullary sinuses, and frozen in dry-ice-cooled isopentane. 16-μm sections were cut on a Leica cryostat (Leica Microsystems). Sections were blocked with 5% goat, donkey, bovine, rat, or rabbit serum and then stained with one or more of the following Abs: ZIKV NS2b protein Ab (polyclonal, Genetex), ZIKV E protein Ab (polyclonal, Genetex), ERTR7 (rat monoclonal, Abcam), B220 (clone RA3-6B2, Thermo Fisher Scientific), CD169 (clone 3D6.112, BioLegend), Lyve-1 (clone ALY7, Thermo Fisher Scientific), CD11c (clone N418, Thermo Fisher Scientific), SIGN-R1 (clone eBio22D1, Thermo Fisher Scientific), CD31 (clone MEC13.3, BioLegend). Sections were incubated with secondary antibodies as needed and as controls, and images were acquired on a Leice SP8 microscope using identical PMT (photomultiplier tube) and laser settings. Images were processed and analyzed using Imaris software (Oxford Instruments).

QUANTIFICATION AND STATISTICAL ANALYSES

Significances were calculated using Prism V 8.3.0 (Graphpad Software) using unpaired two-tailed Mann-Whitney t-tests (when only two groups were present) or using a one-way ANOVA as indicated in the Figure legends.